Draft version August 19, 2016
Preprint typeset using LaTeX style AASTeX6 v. 1.0

USING ICE AND DUST LINES TO CONSTRAIN DISK SURFACE DENSITY

Diana Powell[1,2], Ruth Murray-Clay[1], and Hilke E. Schlichting[3]

[1]Department of Astronomy and Astrophysics, University of California, Santa Cruz, CA 95064
[2]dkpowell@ucsc.edu
[3]Department of Earth, Atmospheric and Planetary Sciences, Massachusetts Institute of Technology, 77 Massachusetts Avenue, Cambridge, MA 02139

ABSTRACT

The total disk surface density is a fundamentally defining feature of protoplanetary disks. We present a novel method for determining the total disk surface density through assuming that the process of particle drift controls the radial scale of the disk. We use TW Hydra as our fiducial disk and find that the disk size and ice line locations can be accurately reproduced using a simplified self consistent model that relies on the disk surface density derived from the 'dust lines' which indicate the disk radial scale at different observational wavelengths. We apply our simplified model to a large disk parameter space and find several observational diagnostics of our physical assumptions. In particular, we predict that across a given CO fraction we should find that disks with large radial scales have shorter ice lines. We also provide an updated and expanded method of determining the impact of drift in modeling the molecular ice lines in a disk.

Keywords: astrochemistry: circumstellar matter: molecular processes

1. INTRODUCTION

Since the first protoplanetary disk was discovered observationally, astrophysical disk research has played an important role in understanding stellar evolution and planet formation (O'dell et al. 1993; review by Shu et al. 1987). The discovery of planets around other stars (exoplanets) has sparked further interest in the study of disks for one compelling reason: other planetary systems do not resemble our own (see reviews by Howard 2013 and Fischer et al. 2014). The accepted solar nebula theory of planet formation that accurately explains our solar system fails to adequately explain other systems without modification (review by Benz et al. 2014). This realization has lead to the idea that planet formation is chaotic and depends strongly on the initial conditions of the system.

The immediate initial conditions of planet formation are encapsulated in the protoplanetary disk that surrounds the young star. We are currently in an era dominated by unprecedented telescopic advances that allow us to observe disks directly (i.e. the Atacama Large Millimeter Array, ALMA). These advances have given us many insights into the complexity and variety of protoplanetary disks (see reviews by Williams & Cieza 2011 or Andrews 2015). Many disk characteristics, however, remain largely unconstrained. In particular, fundamental disk properties such as the total surface density and chemical composition are not well determined for a large population of disks and consequently the physical processes that dominate disk properties have not been well determined and tested.

The total surface density of disks is a fundamental property that is crucial in disk interpretation. Observational constraints of this important property have recently been called into questioned and could be entirely unconstrained (Mundy et al. 1996, Andrews et al. 2009, 2010b; Isella et al. 2009, 2010a; Guilloteau et al. 2011; etc.). Given these uncertainties, we adopt an agnostic point of view in regards to surface density and derive this quantity using a novel method. In particular, we focus on using this novel estimate of disk surface density to theoretically derive observational diagnostics of disk properties that focus on the current to near future observational capabilities. These observational diagnostics could function as probes of underlying physics that aid in further disk modeling. We can maximize the effectiveness of these diagnostics by starting with observations that are not well understood and using physical assumptions to generalize these trends to other systems.

We use two sets of observations to constrain disk surface density with little prior assumption. The first is a set of recent observations, using the Jansky Very Large Array (JVLA) and the sub-millimeter array (SMA), of TW Hydra that demonstrate that the disk radial scale is distinctly smaller at longer wavelengths (Menu et al. 2014, Cleeves et al. 2015, Andrews et al. 2012). These

observations provide information about the distribution of dust grains throughout the disk. We are also able to directly observe disk chemistry as well as disk radial scale using ALMA. This is done through direct measurements of CO gas line emission or through the indirect measurement of the CO ice line through the observation of the N_2H^+ ion which is only present in large abundance when CO freezes out. The indirect CO ice line measurement has been done for TW Hydra and has a measured location of $\sim$ 30 AU (Qi et al. 2013). Direct observations of CO have also been done for TW Hydra and give insight into the surface density contributed by CO which is a temperature dependent quantity (Cleeves et al. 2015; Rosenfeld et al. 2012).

We begin this paper by discussing representative parameters for our fiducial disk, TW Hydra, in Section 2. We next detail the framework for our modeling in Section 3. In Section 4 we present our modeling results for TW Hydra and our application to a larger range of disk parameter space. We conclude with a paper summary and a discussion of the presented observational diagnostics in Section 5.

2. PARAMETERS FOR FIDUCIAL DISK TW HYDRA

To aid in the discussion of our disk modeling we consider TW Hydra as our fiducial disk.

TW Hydra is a bright, long-lived, nearby disk (Rhee et al. 2007). Although it is not representative of the typical disk, it serves as a useful test case due to the comparative ease of observations. We adopt a temperature profile for TW Hydra assuming passive stellar heating following Chiang & Goldreich (1997) where the canonical temperature profile is :

$$T(r) = T_0 \times r^{-3/7} \tag{1}$$

where the coefficient T_0 is a function of stellar luminosity and stellar mass defined at 1 AU and is determined via:

$$T_0 = L_\star^{2/7} \left(\frac{1}{4\sigma_{SB}\pi}\right)^{2/7} \left(\frac{2}{7}\right)^{1/4} \left(\frac{k}{\mu G M_\star}\right)^{1/7}. \tag{2}$$

We adopt the following parameters for TW Hydra: $L_\star = 0.28 L_\odot$, $M_\star = 0.8 M_\odot$, $\mu = 2.3 \mathrm{m_H}$ assuming a hydrogen/helium disk composition (Rhee et al. 2007). Using this equation we derive $T_0 \sim 90$ K and a total disk temperature profile of:

$$T(r) = 90 \times r^{-3/7} \tag{3}$$

There has been great success modeling disks using the following surface density profile reviewed in Andrews 2015:

$$\Sigma(r) = \Sigma_c \left(\frac{r}{r_c}\right)^{-\gamma} \exp\left[-\left(\frac{r}{r_c}\right)^{2-\gamma}\right] \tag{4}$$

This profile is a shallow power law at small radii and follows an exponential fall off at radii larger than the critical radius. For TW Hydra the best fit parameters are a critical radius $r_c = 30$ AU, $\gamma = 1$, and $\Sigma_c \sim 0.4$ given the disk parameters from Rosenfeld et al. 2012 based on measurements of CO line emission and a CO fraction of 1.4×10^{-4} $\mathrm{n_H}$ (Pontoppidan 2006).

While this surface density normalization accurately reproduces the observations, there is evidence that it might not be correct. This surface density normalization is based off of a CO line emission measurement and an assumed CO fraction. Recent observations indicate that the generally assumed CO fraction is likely incorrect in at least some cases and TW Hydra in particular (Schwarz et al. 2016: Bergin et al. 2013).

TW Hydra also has a measured accretion rate of $\sim 10^{-9}$ $\mathrm{M_\odot\ yr^{-1}}$ (Gunther et al. 2015). We can use the surface density from expression to determine an approximation for mass accretion rate:

$$\dot{M} = \frac{M_{\rm disk}}{t_{\rm disk}} \tag{5}$$

where $\dot{M}$ is the mass accretion rate, $t_{\rm disk}$ is the age of the disk (roughly 8 Myr for TW Hydra: Bell et al. 2015), and $M_{\rm disk}$ is the disk mass which we take to be the mass of TW Hydra interior to the cut off radius of 30 AU (Jones et al. 2012). We adopt this estimate for $\dot{M}$ as reasonable for young disks as, for simple viscous disk models, disk age is proportional to the age of the accretion disc with a proportionality constant of order unity. We can thus regard disk age as a proxy for disk evolution timescale and use this simple dimensional argument. Equation 5 gives an accretion rate that is 3 order of magnitudes smaller than the observationally measured accretion rate for TW Hydra.

These surface density complications thus motivate a more agnostic treatment of the surface density profile.

3. MODEL FRAMEWORK

We present our simplified methods of modeling protoplanetary disks with the goal of determining observational diagnostics of fundamental physical process and disk properties. As we present these methods we use TW Hydra as an illustrative example. Modeling TW Hydra is particularly useful as we already know the location of the dust and ice lines. TW Hydra therefore provides the obvious test of our physical assumptions and whether or not they are widely applicable to other disks.

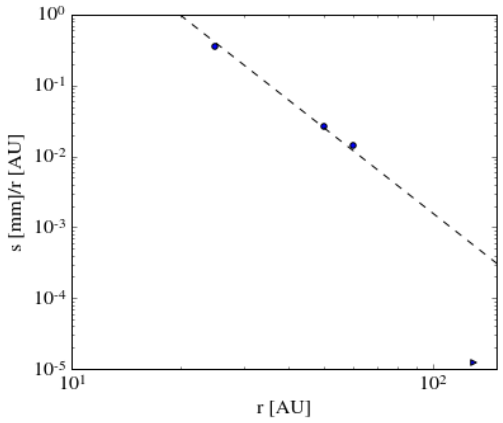

Figure 1. The dominant particle size divided by the disk radius as a function of radius. The three blue circles are observations from Menu et al. 2014, Cleeves et al. 2015, and Andrews et al. 2012. The upper limit arrow represents measurements of the CO gas and might be indicative of the total size of the disk (Debes et al. 2013).

In Section 3.1 we discuss our modeling of disk *dust lines* which we use to refer to the disk radial scale dominated by a particular dust grain size. These dust lines were observed in TW Hydra which we discuss further in Section 3.1. We continue to discuss the relevant physics in our model in Section 3.2 as we discuss our modeling of disk ice lines.

3.1. *Dust Lines*

As mentioned in Section 1, the radial scale of TW Hydra appears smaller when observed at longer wavelengths. Observations at 0.87 mm show a disk size of approximately 60 AU (Andrews et al. 2012), at 1.3 mm the disk size is around 50 AU (Cleeves et al. 2015), and at 9 mm the disk size is approximately 25 AU (Menu et al. 2014). If we assume that the radiation at these wavelengths is dominated by the largest particles in the size distribution then these observations give us information about the distribution of dust particles throughout the disk (Birnstiel & Andrews 2015). In particular, we assume that the wavelength of the observations is equivalent to the dominant particle size at the largest radius observed as shown in Figure 1. When we plot the particle size as a function of radius we see that this points are well fit by a power law function.

Our primary assumption in modeling the disk dust lines is that their location is dominated *entirely* by particle drift. To do this we consider the distance that a particle would drift over the lifetime of the disk. A number of timescale could impact the dust line locations such as drift, growth, and collisional destruction. We consider the regime dominated by drift as motivated in Powell, Murray-Clay, & Schlichting (in prep).

3.1.1. *Radial Drift*

In a protoplanetary disk the gas orbits at a sub-Keplerian velocity due to an outward pressure gradient (Weidenschilling 1977). The particles in the disk continue to rotate at a Keplerian velocity ($v_k \equiv \Omega_k r$) and experience a headwind from the gas. This headwind causes the particles to loose angular momentum and drift radially inwards ((Weidenschilling 1977;Takeuchi & Lin 2002). The amount of drift that a particle experiences depends on how well-coupled the particle is to the gas. This gas and particle coupling can be quantified by a dimensonless stopping time: $\tau_s \equiv \Omega_k t_s$ where t_s is defined as:

$$t_s = \begin{cases} \rho_s s/\rho c_s & s < 9\lambda/4 \text{ Epstein drag,} \\ 4\rho_s s^2/9\rho c_s \lambda & s > 9\lambda/4, \mathrm{Re} \lesssim 1 \text{ Stokes drag.} \end{cases} \tag{6}$$

as summarized in Chiang & Youdin 2010. Here ρ is the gas midplane density, $\rho_s = 2$ g cm^{-3} is the density of a solid particle, s is the particle size, and λ is the gas mean free path.

The particle drift velocity is:

$$\dot{r} \approx -2\eta\Omega_k r \left(\frac{\tau_s}{1+\tau_s^2}\right) \tag{7}$$

where $\eta \approx \frac{c_s^2}{2v_k^2}$ (from the review by Chiang & Youdin 2010) and we define the drift timescale as:

$$t_{\mathrm{drift}} = \left|\frac{r}{\dot{r}}\right| \tag{8}$$

We can now derive an equation for drift timescale that directly depends on the disk surface density. We do this by realizing that the parameter we define as $v_0 \equiv \eta v_k = \frac{c_s^2}{2v_k}$ varies weakly with radius. We find that $c_s \propto r^{-3/14}$ where $c_s = \sqrt{\frac{kT}{\mu}}$ using equation 3 for temperature as a function of radius. For the Keplerian velocity we find that $v_k \propto r^{-1/2}$ using Kepler's third law. This gives a parameter v_0 that is weakly dependent on radius: $v_0 \propto r^{1/14}$.

When deriving the surface density based off of the dust line measurements we consider a small dimensionless stopping time due to the small particle sizes inferred from dust line observations (see Section 3.1). In the outer disk where we observe these dust lines small bodies are in the Epstein drag regime and are well coupled to the gas. We therefore rewrite the dimensionless stopping time from Equation 6 in the Epstein regime as $\tau_s = \frac{\rho_s s}{\Sigma}$. This allows us to write the drift timescale directly in terms of the surface density, radius, particle size, and

the parameter v_0:

$$t_{\rm drift} = \frac{\Sigma r}{v_0 \rho_s s} \quad (9)$$

This new formulation of the drift timescale allows us to set the drift timescale equal to the age of the disk and solve for surface density at the dust line radius. We do this assuming that the dominant particle size s is given by the wavelength of the observation. We thus derive the following equation for disk surface density as a function of radius.

$$\Sigma(r) = \frac{t_{\rm disk} v_0 \rho_s s}{r} \quad (10)$$

where $t_{\rm disk}$ is the age of the system. This formulation is particularly valuable as it gives a direct scaling between surface density and radius as the term v_0 is roughly constant with radius. This direct relation only needs a further assumed temperature profile to derive the disk surface density.

We can now use Equation 10 to determine the surface density of TW Hydra as a function of radius (See Figure 2). We again use a disk age ($t_{\rm disk}$) of 8 Myr.

The derived surface density points are well described by steep power law of approximately r^{-4}. Initially, this appears to be an unrealistically steep function. However, as these points fall close to the observational fall-off range of the Rosenfeld et al. 2012 disk, they match the profile well when a surface density normalization factor is applied.

We treat the critical surface density Σ_c as a floating parameter used to normalize the Rosenfeld et al. 2012 surface density to fit our derived surface density points (see Figure 2). This gives a close fit to our rough surface density approximation because the exponential fall off occurs close the the smallest radii we consider. We find that a surface density normalization of $\Sigma_c = 10^3$ adequately matches our derived surface density points. We are currently investigating the effect of error bars on dust line radial measurements.

3.1.2. *Particle Growth*

As discussed in Powell, Murray-Clay, & Schlichting (in prep), the growth of particles is something that could change this simplified picture of particle drift. In the drift regime that we consider, larger particles drift faster and do not remain at the same dust location for long timescales. Thus, we assume that the particle size that contributes the most to emission is the largest particle at that radius that has not yet had time to drift further inwards. This is particularly true as dynamical timescales in the outer disk are slower due to the decreased surface density. A more thorough treatment of growth might change this picture and we plan on quantifying this effect further.

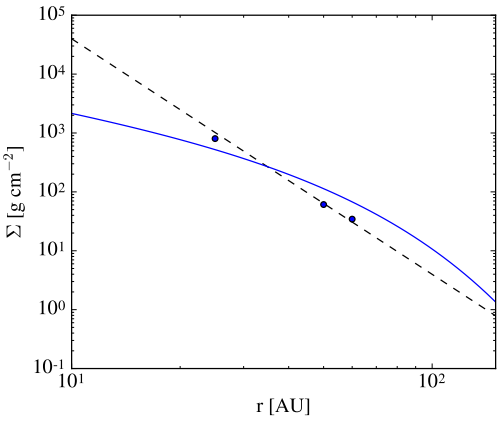

Figure 2. The points indicate the surface density of TW Hydra derived using the three observational data points. The surface density profile at these radii are well fit by a dramatic r^{-4} power law. The normalized surface density profile is shown in blue. The normalized surface density profile is an r^{-1} power law interior to the critical radius (r_c) of 30 AU and is then described by an exponential fall off at radii larger than r_c. We find that a surface density normalization of $\Sigma_c = 10^3$ adequately matches our derived surface density points.

3.2. *Ice Lines*

Ice lines are the points in a disk where the temperature changes such that volatile compounds freeze out at radii past this point (Hollenbach et al. 2009). The three ice lines that are most frequently calculated are H_2O, CO_2, and CO as these species are considered to be in relatively high abundance (Oberg et al. 2011). To date, only the CO ice line has been observed (Qi et al. 2013). We thus primarily focus on CO ice line calculations. However, when we consider a larger parameter space of disk parameters, we further extend our arguments to other volatile species as well.

There are three theoretical pieces of physics that we consider in our ice line calculations: adsorption, desorption, and drift.

3.2.1. *Volatile Adsorption and Desorption*

The classic ice line calculation balances adsorption and desorption flux onto a grain to determine the ice line radius (Hollenbach et al. 2009; Oberg et al. 2011). We refer to this ice line as the 'classical ice line'. Following Hollenbach et al. 2009, these two fluxes are quantified as:

$$F_{\rm adsorb} \sim n_i c_s \quad (11)$$

$$F_{\rm desorb} \sim N_{s,i} \nu_{\rm vib} {\rm e}^{-E_i/kT_{\rm grain}} f_{s,i} \quad (12)$$

where n_i is the relevant gas density species, c_s is the sound speed, $N_{s,i} \approx 10^{15}$ sites cm^{-2} is the number of adsorption sites per volatile per cm^2, $\nu_{\rm vib} = 1.6 \times 10^{11} \sqrt{(E_i/\mu_i)}$ s^{-1} is the molecules vibrational frequency in the surface potential well, E_i is the adsorption binding energy in units of Kelvin, $f_{s,i}$ is the fraction of the surface adsorption sites that are occupied by species i (which we take to be unity). Finally, we assume that $T_{\rm grain} = T$, meaning that the dust and gas have the same temperature in the disk mid-plane.

Balancing Equations 11 and 12 allows for us to solve for the freezing temperature of a species as a function of radius for a given disk surface density profile. We then locate the classical ice line location by finding the disk radius where the molecular freezing temperature is equal to the disk temperature at that location. This self-consistent solving of the classical ice line location allows us to determine how the ice line location changes as a function of both disk surface density and temperature.

3.2.2. *The Influence of Particle Drift*

Particle drift, as described in Section 3.1.1, influences the location of the ice lines (Piso et al. 2015). This is because particles that drift faster can cross the ice-line before desorbing, thus potentially moving the location of the ice line inwards. The drift ice line location can be calculated by setting the desorption timescale equal to the drift timescale and solving for the desorption distance, $r_{\rm des}$ (as verified by time evolving calculations in Piso et al. 2015). This is done analytically for the small stopping time approximation in the Piso et al. 2015 Appendix. We extend this calculation to the $\tau_s > 1$ regime. We balance the drift timescale (Equation 8) and the desorption timescale (Equation 13) to solve for $r_{\rm des}$.

$$t_{\rm des} = \frac{\rho_s}{3\mu_i m_{\rm H}} \frac{s}{N_{s,i}\nu_{\rm vib} {\rm e}^{-E_i/kT_{\rm grain}}} \tag{13}$$

where $\dot{r}$ is given in Equation 7 and μ_i is the molecular weight of the desorbing species.

Again, we make no approximations in Equation 8 in regards to τ_s. We instead use the two distinct stopping time expressions given both Stokes and Epstein regimes.

We use the iterative numerical modification of the Powell hybrid method (see MINPACK subroutine HYBRD) to solve for radius through balancing Equations 8 and 13. We consider the radial dependence of each term without approximation which allows us to derive a completely self-consistent estimate of $r_{\rm des}$ for any arbitrary surface density or temperature profile.

We compare the difference between the drift ice line and the classical ice line for our new self-consistent solver and the analytic solver from Piso et al. 2015 in Figure 3. Figure 3 considers CO molecules located at the classical CO ice line for the disk parameters from Piso et al. 2015.

We find that particles smaller than 8 cm do not drift past the ice line. Particles larger than 8 cm do experience drift in this case, with the maximum drift reached at a τ_s of around 1 that reaches a near constant value at higher stopping time. The nearly constant drift distance at particle sizes with a stopping time greater than 1 occurs due to the interplay between two different pieces of physics. The first is that the larger the particle size the longer it takes for that particle to desorb and the further it can drift past the ice line. The second is that the maximum drift velocity occurs for particles with $\tau_s = 1$.

The decrease in drift velocity past a stopping time of one is offset by the increase in particle size until the regime changes from Stokes to Epstein. We therefore see a functionally constant $r_{\rm des}$ for large particle sizes.

Due to this effect, we consider the drift ice line of a $\tau_s = 1$ particle at the classical ice line location and numerically solve for the drift distance without making any further approximations. This is roughly indicative of the largest drift distance past the ice line as particles above a certain size all desorb at roughly the same distance. The existence of a maximum drift distance found in our self-consistent solution is important in understanding the relevance of particle drift in ice line calculations. Given this updated calculation we can now determine when drift will play a distinct role in determining the location of the ice line.

We find that the particular radial location of the classical ice line in a disk strongly impacts the importance that drift will play in altering ice line observations. We find that the process of drift becomes important when the classical ice line occurs at a point in the disk where larger particles have a stopping time close to 1 (see Figure 4). Drift will play the largest role at the radial location where the particle size with $\tau_s = 1$ reaches a maximum. Recall that the $\tau_s = 1$ particle is roughly indicative of the largest drift distance past the ice line.

While this general point is always true, the size of the $\tau_s = 1$ particle at a particular location changes depending on the overall surface density profile and the radius that is considered. Thus, in every disk, there is a radial location where the $\tau_s = 1$ particle size reaches a maximum. If the ice line of a particular molecule occurs near this point then drift will play a large role in determining the true ice line location.

3.3. *CO Fraction*

Given our physical setup, we can now determine the CO fraction if the radial size of the disk and the CO ice line are both known observational quantities. This is done by scaling our classical CO ice line as described in section 3.2.1 to determine a CO surface density. We then divide the CO surface density by the derived total surface density as described in Section 3.1.1.

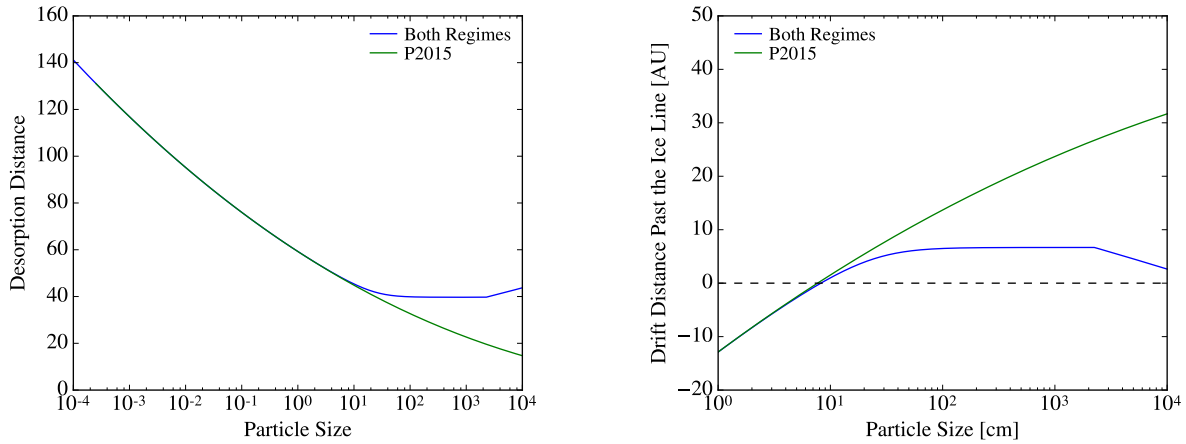

Figure 3. Left: The drift distance for CO molecules calculated using the analytic method from Piso et al. 2015 (green) and our new extended solver (blue). We find great agreement for particles with a stopping time less than unity. Right: The distance that a CO particle is able to drift past the classical CO ice line before desorbing using the analytic method from Piso et al. 2015 (green) and our new self-consistent solver (blue). Using our extended solver we see that for this comparison case, particles smaller than 8 cm do not drift past the ice line. Particles larger than 8 cm do experience drift in this case, with the maximum drift reached at a τ_s of around 1 that reaches a constant value at higher stopping time.

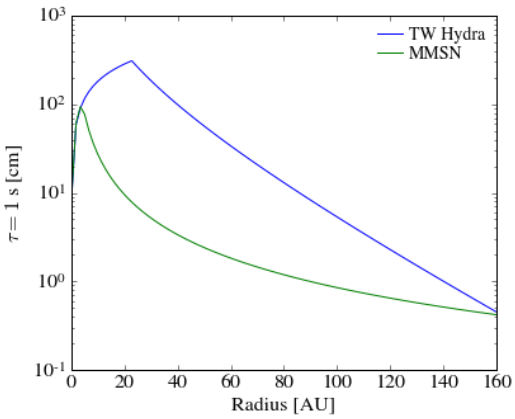

Figure 4. The size of $\tau_s = 1$ particles in the disk as a function of radius for two different surface density profiles: our TW Hydra surface density profile (blue) and the commonly used minimum mass solar nebula surface density profile (green). The τ_s particles are the largest particles that are still well-coupled to the gas. Drift plays the largest role in shifting the ice line locations when the ice lines occur close to the peak in these functions as large particles desorb slower.

The fraction of CO (X_{CO}) in the disk is not well constrained for TW Hydra. The commonly used literature value of CO for disks is $0.9 - 2 \times 10^4$ n_H (Pontoppidan 2006). However, recent observations of TW Hydra quote an upper limit of $\sim 10^{-6}$ n_H (Schwarz et al. 2016) through considering only the hot gas in the disk.

We derive a CO fraction using the CO ice line observed in Qi et al. 2013 and our total surface density determined in Section 3.1.1. We find a CO fraction of approximately 10^{-7} n_H. This fraction is consistent with the conclusion from Schwarz et al. 2016. The reduction of 3 orders of magnitude from the commonly accepted literature value for disks indicates that other processes in the disk, such as photochemistry, must be playing an important role.

4. RESULTS

We are now able to test our physical assumptions through applying our physical model to TW Hydra and comparing to the fitted observations as a proof of concept. We then apply these assumptions to a broader range of parameter space to derive general trends and observational diagnostics.

4.1. *Complete Application to TW Hydra*

We are now able to completely model TW Hydra using an X_{CO} of 10^{-7} and a surface density normalization of $\Sigma_c = 10^3$ (see Figure 5). We find that we are able to adequately reproduce the observed disk radial scale of TW Hydra at various wavelength by assuming that the drift timescale is equal to the age of the system and using our derived surface density profile (see Section 3.1.1). We recalculate our classical CO ice line following Section 3.2.1 and find that it is in great agreement with the observed ice line of ~ 30 AU as expected (Qi et al. 2013). We also find the same CO fraction through using the quote CO surface density from Schwarz et al. 2016 in comparison to our derived total disk surface density.

We calculate the maximum CO drift ice line following Section 3.2.2 and find that the drift ice line for TW Hydra is distinctly interior to the classical CO ice line. The radius of the maximum drift location is close to the ~ 17 AU mid plane CO ice line as derived by Schwarz et al. 2016, although these measurements might not be strictly analogous.

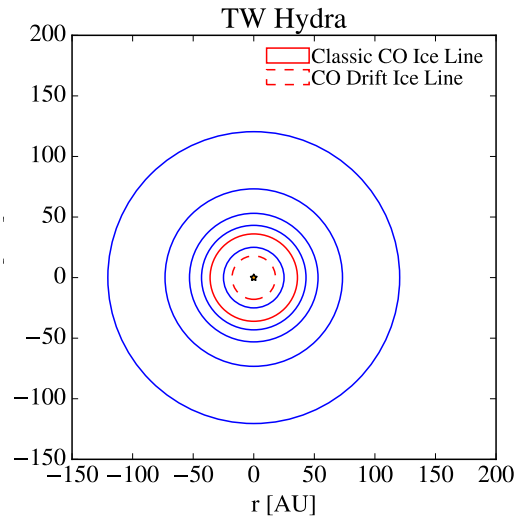

Figure 5. A model of the dust and ice lines in TW Hydra. The blue lines are the dust lines solved by assuming that the drift timescale is equal to the age of the system. These blue lines adequately reproduce the observed disk radial scale of TW Hydra at various wavelengths. The solid red line is the classical CO ice line solve by balancing the adsorption and desorption flux onto a grain. This line is in great agreement with the observed ice line of $\sim$ 30 AU (Qi et al. 2013). The dashed red line is the CO drift ice line for a $\tau_s = 1$ particle. This ice line roughly corresponds to the measured mid plane CO snow line of $\sim$ 17 AU from Schwarz et al. 2015 although this may not be an entirely analogous comparison.

We can now consider the accretion rate for our newly normalized surface density profile for TW Hydra using Equation 5. We find an accretion rate of $\sim 10^{-8}$ $M_\odot$ yr^{-1}. This accretion rate is an order of magnitude larger than the measured accretion rate for TW Hydra of $\sim 10^{-9}$ $M_\odot$ yr^{-1} (Gunther et al. 2015). This is an improvement from the previous surface density profile that gives a value that is 3 orders of magnitude too small. However, we are currently investigating error bars on the radial scales of TW Hydra to determine the reasonableness of our derived accretion rate.

After completely modeling TW Hydra using our simplified physical model we find that the disk size of TW Hydra can be reproduced by assuming $t_{\rm drift} = t_{\rm disk}$. We also find that the CO ice line locations can be accurately determined by self-consistently balancing adsorption and desorption while considering particle radial drift.

While we fit these parameters to observations for TW Hydra we are nonetheless able to show that dust lines give an indication of the total disk surface density. We also demonstrate that using our derive surface density profile, when coupled to observed ice line measurements, we are able to derive the CO fraction using self-consistent modeling.

4.2. *Observables in Other Disks*

We now apply our model more generally to determine how the classical and drift ice line locations scale with disk surface density and temperature. We consider a large range of parameter space as it is possible that disk parameter space for different stellar types is larger than was previously assumed. We also look in more detail at the case of an early sun-like star to determine how disk size and ice line locations change with disk surface density to form an intuition for observable diagnostics of the physics that we have considered.

4.3. *Ice Lines as a Function of Disk Surface Density and Temperature*

We self-consistently solve for the difference between the classic and drift ice lines for CO, CO_2, and H_2O (see Figure 6). We use the fraction of these molecules as used in Oberg et al. 2011: $X_{CO} = 1.5 \times 10^{-4}$ n_H, $X_{CO_2} = 0.3 \times 10^{-4}$ n_H, and $X_{H_2O} = 0.9 \times 10^{-4}$ n_H. Assuming these molecular fractions, we find that drift is most important for CO_2 and generally increases at moderate densities and high temperatures for all three molecular species. Here we consider a disk passively heated by the star as discussed in Chiang & Goldreich 1997 for a fixed snapshot in time (accretion heating and stellar luminosity changes are not considered). The temperature profile used is given in Equation 1 for different temperature normalizations (T_0).

We find that drift is most important for CO_2. This finding is reasonable given our discussion in Section 3.2.2 as CO_2 has a freezing temperature that is warmer than CO and cooler than H_2O. The location of the classical CO_2 ice line is thus generally located in the middle of the disk near the peak in $\tau_s = 1$ particle size meaning that we expect drift to play a large role (see Figure 3).

We also find that the importance of drift generally increases at moderate densities and high temperatures for all three molecular species. And, most importantly, we find that the disk ice line locations and influence of drift largely depend on the fundamental properties of the disk. This is important to consider when interpreting observations as it allows us a means to derive disk properties from ice line measurements assuming a set molecular fraction.

4.4. *Disk Radial Scale as a Function of Disk Surface Density*

Let us now consider the case of a particular stellar type to aid in intuitively understanding how the dust and ice line locations change as a function of surface density. This is particularly relevant in determining observational diagnostics as these two parameters do not scale with density in the same way.

We consider the case of a sun-like star in more detail to observe trends as a function of surface density alone at a

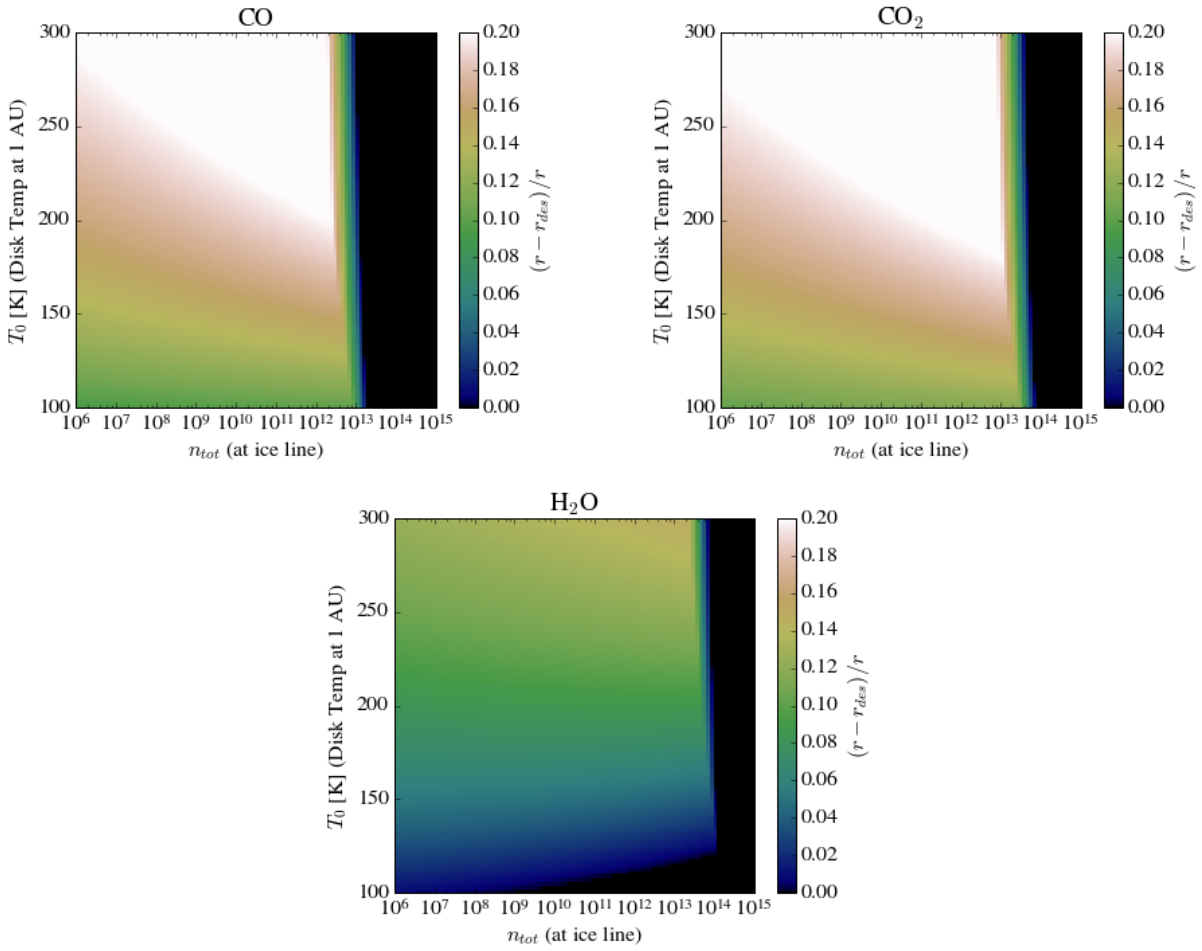

Figure 6. The fractional difference between the classically derived ice line r and the drift ice line r_{des} as a function of disk density and temperature. Drift is most important for CO_2 and generally increases at moderate densities and high temperatures. The y-axis label T_0 refers to the temperature normalization for Equation 1.

fixed temperature profile. We again choose the familiar $r^{-3/7}$ temperature profile of a passively irradiated disk and normalize this function so that the minimum mass solar nebula has a classic H_2O ice line outside of 1 AU (see Figure 7 and Section 3.2.1). We do this relying on the evidence that the Earth is not an ice ball and thus must have formed interior to the H_2O ice line.

The derived temperature profile is:

$$T = 210 \times r^{-3/7} \quad (14)$$

We again assume CO, CO_2, and H_2O abundances as assumed in Oberg et al. 2011.

We find that for both CO and CO_2, the disk size increases with increasing surface density while the ice line decreases (see Figure 8). For the CO ice line, the drift distance is negligible. For the CO_2 ice line drift plays a small role that decreases in importance with increasing surface density (see Figure 8). The trends for the H_2O ice line are the same as for the CO ice line where the ice line drift distance is negligible.

These trends are the observational diagnostics needed to determine the accuracy of our physical assumptions.

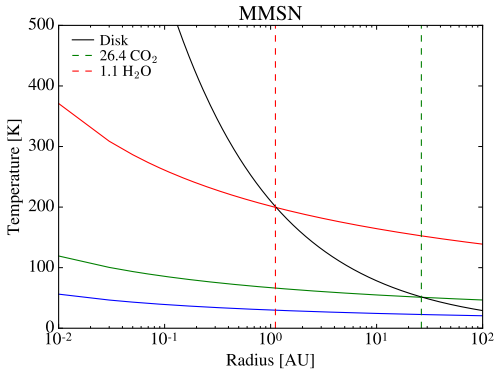

Figure 7. The H_2O (red), CO_2 (green), and CO (blue) freezing temperature as a function of radius for the minimum mass solar nebula (MMSN). The black line is the minimum temperature profile that places the H_2O ice line outside of 1 AU.

5. SUMMARY AND DISCUSSION

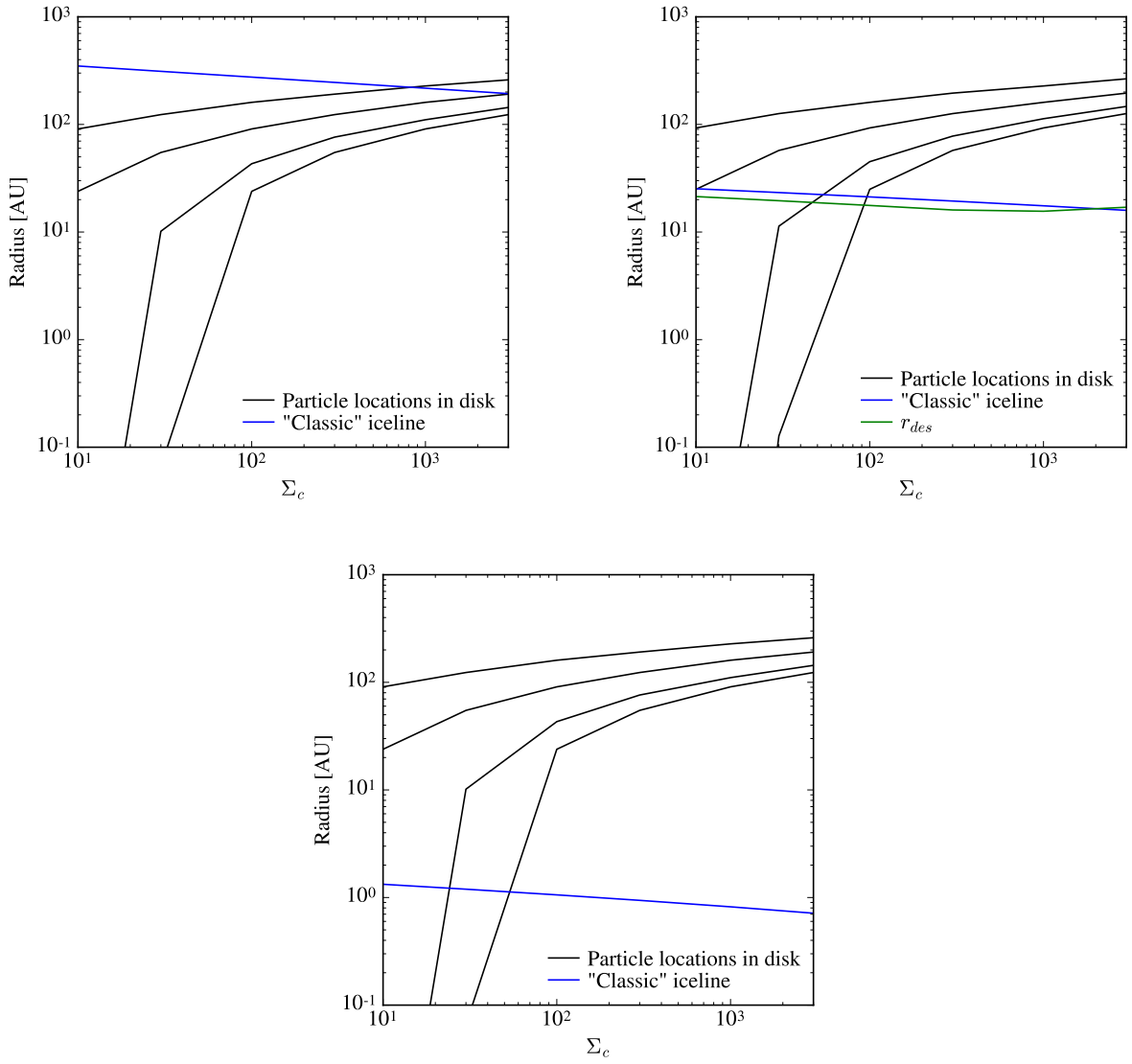

Figure 8. The disk radial scale for different particle sizes (black lines), the classically derived ice line locations (blue line) and the drift ice line (green line) for CO (top right), CO_2 (top left), and H_2O (bottom middle) as a function of surface density. The radial size of the disk increases dramatically with increased surface density while the ice line location decreases.

We begin the discussion of our observationally motivated simplified disk model with the decision to be agnostic about the disk surface density profile. We use TW Hydra as an illustrative example and as a proof of concept. We use the locations of dust lines to determine the disk surface density by setting $t_{\rm drift} = t_{\rm disk}$. We then obtain a larger surface density normalization for TW Hydra than was found in the literature by Rosenfeld et al. 2012.

Our new surface density gives an accretion rate measurement that is 1 order of magnitude too high as compared to 3 orders of magnitude too low using the previous surface density normalization. We expand the calculations for the drift ice line of disks and expand the calculation to self-consistently include particles with dimensionless stopping time greater than one. We calculate a CO fraction for TW Hydra of 10^{-7} $M_\odot$ yr^{-1} which is two orders of magnitude lower than the standard literature value, however, this is consistent with derived values of TW Hydra as seen in Schwarz et al. 2016.

We demonstrate that our simple model applied to a large parameter space indicates that both the ice line locations and the importance of drift in the ice line interpretation depends on both disk density and temperature. We also demonstrate that for a fixed stellar type, the disk ice lines decrease in radius as the disk radial scale increases.

To test the dominant physics in our simplified model it is necessary to analyze dust and ice line observations for a large number of disks. The observational diagnostics

of our model predict that we should find that disks with larger dust lines have smaller ice lines.

We expect this trend to be particularly true across a single stellar type. This is because we can likely assume that the CO fraction is constant across a stellar type if this ratio is primarily determined by photochemistry or other stellar dependent processes. This assumption would allow us to accurately understand and test expected trends across a particular set of assumptions.

There are many exciting modeling outcomes if our observational diagnostics prove to be correct. If true, we will be able to glean an estimate of the total disk surface density from the disk radial scale alone. We will also be able to quickly determine the CO fraction from the CO ice line location and the density derived from the disk radial scale. This information would be invaluable for other disk modeling and the further understanding of planet formation and evolution.

6. ACKNOWLEDGEMENTS

This work was done as a part of the Kavli Summer Program in Astrophysics: Exoplanetary Atmospheres 2016. We would like to thank Jonathan Fortney and Pascale Garaud for providing us with the opportunity to work together on this project and for organizing a wonderful workshop. We thank James Owen for his useful comments and insightful discussion. This material is based upon work supported by the National Science Foundation Graduate Research Fellowship under Grant DGE1339067.

REFERENCES

Andrews, S. M. 2015, PASP, 127, 961
Andrews, S. M., Wilner, D. J., Hughes, A. M., Qi, C., & Dullemond, C. P. 2009, ApJ, 700, 1502
Andrews, S. M., Wilner, D. J., Hughes, A. M., Qi, C., & Dullemond, C. P. 2010, ApJ, 723, 1241
Andrews, S. M., Wilner, D. J., Hughes, A. M., et al. 2012, ApJ, 744, 162
Bell, C. P. M., Mamajek, E. E., & Naylor, T. 2015, MNRAS, 454, 593
Benz, W., Ida, S., Alibert, Y., Lin, D., & Mordasini, C. 2014, Protostars and Planets VI, 691
Bergin, E. A., Cleeves, L. I., Gorti, U., et al. 2013, Nature, 493, 644
Birnstiel, T., & Andrews, S. M. 2014, ApJ, 780, 153
Chiang, E. I., & Goldreich, P. 1997, ApJ, 490, 368
Chiang, E., & Youdin, A. N. 2010, Annual Review of Earth and Planetary Sciences, 38, 493
Cleeves, L. I., Bergin, E. A., Qi, C., Adams, F. C., &Oumlberg, K. I. 2015, ApJ, 799, 204
Debes, J. H., Jang-Condell, H., Weinberger, A. J., Roberge, A., & Schneider, G. 2013, ApJ, 771, 45
Fischer, D. A., Howard, A. W., Laughlin, G. P., et al. 2014, Protostars and Planets VI, 715
Guilloteau, S., Dutrey, A., Piétu, V., & Boehler, Y. 2011, A&A, 529, A105
Gunther, H. M., Brickhouse, N. S., Dupree, A. K., et al. 2015, 18th Cambridge Workshop on Cool Stars, Stellar Systems, and the Sun, 18, 231
Hollenbach, D., Kaufman, M. J., Bergin, E. A., & Melnick, G. J. 2009, ApJ, 690, 1497
Howard, A. W. 2013, Science, 340, 572
Isella, A., Carpenter, J. M., & Sargent, A. I. 2009, ApJ, 701, 260
Isella, A., Carpenter, J. M., & Sargent, A. I. 2010, ApJ, 714, 1746
Jones, M. G., Pringle, J. E., & Alexander, R. D. 2012, MNRAS, 419, 925
Menu, J., van Boekel, R., Henning, T., et al. 2014, A&A, 564, A93
Mundy, L. G., Looney, L. W., Erickson, W., et al. 1996, ApJL, 464, L169
Öberg, K. I., Murray-Clay, R., & Bergin, E. A. 2011, ApJL, 743, L16
O'dell, C. R., Wen, Z., & Hu, X. 1993, ApJ, 410, 696
Piso, A.-M. A., Öberg, K. I., Birnstiel, T., & Murray-Clay, R. A. 2015, ApJ, 815, 109
Pontoppidan, K. M. 2006, A&A, 453, L47
Qi, C., Öberg, K. I., & Wilner, D. J. 2013, ApJ, 765, 34
Rhee, J. H., Song, I., Zuckerman, B., & McElwain, M. 2007, ApJ, 660, 1556
Rosenfeld, K. A., Qi, C., Andrews, S. M., et al. 2012, ApJ, 757, 129
Schwarz, K. R., Bergin, E. A., Cleeves, L. I., et al. 2016, ApJ, 823, 91
Shu, F. H., Adams, F. C., & Lizano, S. 1987, ARA&A, 25, 23
Takeuchi, T., & Lin, D. N. C. 2002, ApJ, 581, 1344
Weidenschilling, S. J. 1977, Ap&SS, 51, 153
Williams, J. P., & Cieza, L. A. 2011, ARA&A, 49, 67